Research Square

Preprints are preliminary reports that have not undergone peer review.
They should not be considered conclusive, used to inform clinical practice,
or referenced by the media as validated information.

# Effect of Particle Refinement on Return Loss and Bandwidth Performance of TiCN/$NiFe_2O_4$ Composite Patch Antennas

**N. I. Z. Azman**
Universiti Malaysia Pahang Al-Sultan Abdullah (UMPSA)
**C. D. F. C. Fadzrizal**
Universiti Malaysia Pahang Al-Sultan Abdullah (UMPSA)
**S. Baudha**
BITS Pilani
**M. A. Jusoh**
ashry@umpsa.edu.my

Universiti Malaysia Pahang Al-Sultan Abdullah (UMPSA)

**Research Article**

**Keywords:** Titanium Carbonitride, Nickel Ferrite, Microstrip Patch Antenna, Ball Milling, Calcination; Return Loss, Bandwidth

**Posted Date:** July 13th, 2026

**DOI:** https://doi.org/10.21203/rs.3.rs-9720107/v1

**License:** This work is licensed under a Creative Commons Attribution 4.0 International License.
Read Full License

**Additional Declarations:** No competing interests reported.

**Version of Record:** A version of this preprint was published at Applied Physics A on October 7th, 2026. See the published version at https://doi.org/10.1007/s00339-026-10319-5.

# Effect of Particle Refinement on Return Loss and Bandwidth Performance of TiCN/$NiFe_2O_4$ Composite Patch Antennas

N. I. Z. Azman[1], C. D. F. C. Fadzrizal[1], S. Baudha[2] and M. A. Jusoh[1,*]

[1]Faculty of Industrial Sciences & Technology, Universiti Malaysia Pahang Al-Sultan Abdullah (UMPSA), 26300, Gambang, Pahang, Malaysia

[2]Department of Electrical and Electronics Engineering, BITS Pilani, Goa Campus, Goa, India

*ashry@ump.edu.my

## Abstract

Titanium Carbonitride/Nickel Ferrite (TiCN/$NiFe_2O_4$) composite materials were fabricated for high frequency Microstrip Patch Antenna (MPA) applications through ball milling, calcination, and composite fabrication processes. Titanium Carbonitride (TiCN) powder was subjected to different ball milling durations to reduce particle size and improve particle distribution before composite preparation, while Nickel Ferrite ($NiFe_2O_4$) was synthesized using solid-state reaction followed by calcination at 1100 °C. The structural, morphological, surface, and thermal properties of the synthesized materials were characterized using Particle Sizer, X-ray Diffractometer (XRD), Fourier-transform Infrared Spectroscopy (FTIR), Scanning Electron Microscope (SEM), Brunauer-Emmet-Teller (BET), and Thermogravimetric Analysis (TGA). The results showed that the particle size of TiCN decreased significantly after prolonged ball milling process, while XRD and FTIR analyses confirmed the successful formation of spinel ferrite structure within the composite material. The fabricated TiCN/$NiFe_2O_4$ composite based MPA was evaluated using a Vector Network Analyzer (VNA) within the frequency range of 5 to 20 GHz. The fabricated antennas demonstrated return loss values ranging from -12.0 dB to -42.94 dB with bandwidth values between 0.87 GHz and 3.83 GHz. Sample 4 achieved the best return loss performance of -42.94 dB at 12.53 GHz, while Sample 5 demonstrated dual band operation with the widest bandwidth performance. The obtained findings showed that improved TiCN particle distribution contributed toward better electromagnetic interaction and microwave performance within X band and Ku band frequency regions. Overall, the fabricated TiCN/$NiFe_2O_4$ composite material demonstrated strong potential for high frequency microwave patch antenna applications.

**Keywords:** Titanium Carbonitride, Nickel Ferrite, Microstrip Patch Antenna, Ball Milling, Calcination; Return Loss, Bandwidth

## 1. Introduction

Microstrip Patch Antenna (MPA) has become one of the most widely used antennas in modern wireless communication systems because of its compact structure, low fabrication cost, and easy integration with electronic circuits. MPA is commonly applied in microwave communication systems such as wifi, satellite communication, radar, and internet of things (IoT) devices [1]. The increasing demand for high speed wireless communication and multi frequency operation has encouraged continuous improvement in antenna performance, especially in terms of bandwidth, return loss, radiation efficiency, and operating stability [2]. Conventional copper-based patch antennas provide good electrical conductivity and simple fabrication process. However, copper still has several limitations during high frequency

operation, including narrow bandwidth, poor thermal stability, surface oxidation, and corrosion, which may reduce antenna efficiency and long-term microwave performance [3].

To overcome these limitations, the development of alternative conductive and magnetic materials has become an important approach in antenna research. Material engineering allows antenna performance to be improved through material composition, particle size distribution, and interaction between conductive and magnetic phases without requiring highly complex antenna structures [4]. Conductive ceramic materials and magnetic dielectric materials are especially useful for microwave applications because their electromagnetic properties can influence impedance matching, bandwidth performance, and frequency stability. Therefore, combining conductive and magnetic materials in a composite structure may provide a practical route for improving MPA performance in high frequency regions. The integration of conductive TiCN ceramic particles with magnetic $NiFe_2O_4$ ferrite particles provides a promising strategy for improving electromagnetic interaction within high-frequency microstrip patch antenna structures.

Titanium Carbonitride (TiCN) is a ceramic material known for high electrical conductivity, excellent thermal stability, chemical resistance, and mechanical hardness [5]. These properties make TiCN suitable for applications that require stable behaviour under high frequency and harsh operating conditions. In addition, Nickel Ferrite ($NiFe_2O_4$) is a spinel ferrite material with high magnetic permeability and low dielectric loss, which makes it suitable for electromagnetic and microwave applications. The combination of TiCN and $NiFe_2O_4$ may produce a composite material that contains both conductive and magnetic characteristics. This concept is illustrated in Figure 1, where TiCN particles and $NiFe_2O_4$ particles are combined to form a TiCN-$NiFe_2O_4$ composite with a more integrated and compact structure.

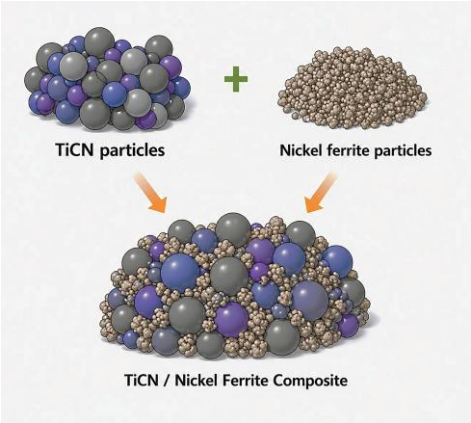



Figure 1. Schematic illustration of TiCN particles, $NiFe_2O_4$ particles, and the formation of TiCN- $NiFe_2O_4$ composite structure

Previous studies have reported the synthesis of TiCN and $NiFe_2O_4$ using different methods, including hydrothermal, sol gel, and solid-state reaction routes [7], [8]. However, many studies mainly focus on individual TiCN or $NiFe_2O_4$ materials, while limited work has been reported on TiCN/$NiFe_2O_4$ composite materials for MPA applications. In addition, the relationship between TiCN particle size reduction, composite microstructure, and antenna electromagnetic performance remains insufficiently explored. Ball milling is a useful mechanical process for reducing particle size and improving powder mixing, while calcination can enhance crystallinity and promote phase formation. The present study emphasizes the influence of TiCN

particle refinement on conductive pathway formation and microwave propagation behaviour within the composite antenna layer. The combination of ball milling and calcination may therefore produce TiCN/$NiFe_2O_4$ composite materials with improved structural stability and more uniform particle distribution [11].

Therefore, this study focuses on the development of TiCN/$NiFe_2O_4$ composite materials for high frequency MPA applications. TiCN powder was subjected to different ball milling durations to investigate the effect of particle refinement, while $NiFe_2O_4$ was synthesized through solid-state reaction followed by calcination. The structural, morphological, surface, and thermal properties of the composite material were analyzed using Particle Sizer, X-ray Diffractometer (XRD), Fourier-transform Infrared Spectroscopy (FTIR), Scanning Electron Microscope (SEM), Brunauer-Emmet-Teller (BET), and Thermogravimetric Analysis (TGA). The fabricated TiCN/$NiFe_2O_4$ composite based MPA was then evaluated using a Vector Network Analyzer (VNA) within the frequency range of 5 to 20 GHz to determine return loss and bandwidth performance. This study is expected to provide a clearer understanding of how TiCN particle refinement and TiCN/$NiFe_2O_4$ composite formation influence microwave antenna performance within X band and Ku band frequency regions. The scope of the present study mainly focuses on the structural characterization and preliminary electromagnetic evaluation of TiCN/$NiFe_2O_4$ composite-based microstrip patch antennas through impedance matching and bandwidth analysis within high-frequency operating regions.

## 2. Materials and Methods

### 2.1 Materials and Chemicals

TiCN powder was used as the main conductive ceramic material in this study. The TiCN powder had a purity of 99.3 % with particle size less than 5 μm. Nickel Oxide (NiO) nanopowder and Iron Oxide ($Fe_2O_3$) powder were used as precursor materials for the synthesis of $NiFe_2O_4$. Polyvinyl Pyrrolidone (PVP) was used as the binder material, while ethanol was used as the dispersion solvent during composite paste preparation. Ferric Chloride ($FeCl_3$) solution was used for the substrate etching process before antenna fabrication.

### 2.2 Preparation of TiCN using Ball Milling

The TiCN powder was processed using a planetary ball milling method to reduce particle size and improve powder uniformity. Approximately 15 g of TiCN powder was mixed with 300 g of steel balls using a powder to ball ratio of 1:20. The milling process was carried out using a Retsch PM 100 Planetary Ball Mill at a rotational speed of 300 rpm. A 30 minutes resting period was applied after every 1 hour of milling to prevent excessive heat generation during the process. Five TiCN samples were prepared based on different milling durations, namely as-milled, 2 hours, 4 hours, 6 hours, and 8 hours, as listed in Table 1. The ball milling machine is shown in Figure 2.

Table 1 Process of Ball Milled TiCN Samples Using Retsch PM 100

| No. of Sample | Ball Mill Time |
|---|---|
| 1 | As-milled |
| 2 | 2 hours |
| 3 | 4 hours |

| | |
|---|---|
| 4 | 6 hours |
| 5 | 8 hours |

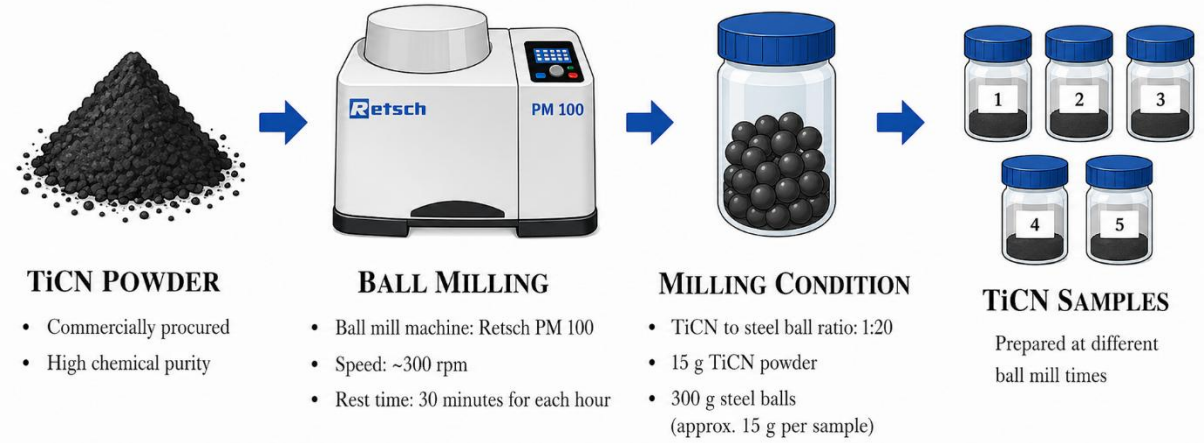



Figure 2. Ball milling process of TiCN powder using Retsch PM 100 Planetary Ball Mill.

### 2.3 Synthesis of $NiFe_2O_4$

$NiFe_2O_4$ powder was synthesized using a solid-state reaction method followed by ball milling and calcination [7]. NiO and $Fe_2O_3$ powders were prepared based on a stoichiometric ratio of 1 mol to 1 mol. Approximately 3.8 g of NiO and 8.2 g of $Fe_2O_3$ were weighed and manually mixed using a mortar and pestle to obtain an initial homogeneous powder mixture. The mixed powder was then transferred into the ball milling container and milled at 300 rpm for 8 hours using a powder to ball ratio of 1:20. Similar to the TiCN milling process, 30 minutes resting period was applied after every 1 hour of milling to reduce overheating. After the milling process, the powder mixture was transferred into a crucible boat and calcined in a laboratory tube furnace at 1100 °C for 6 hours with a heating rate of 10 °C/min. The calcination process was conducted to promote phase formation and improve the crystallinity of $NiFe_2O_4$. After cooling to room temperature, the calcined powder was ground again using a mortar and pestle to obtain fine $NiFe_2O_4$ powder. The preparation of $NiFe_2O_4$ was shown in Figure 3. The reaction involved in the formation of $NiFe_2O_4$ can be represented as:

$$NiO + Fe_2O_3 \rightarrow NiFe_2O_4$$

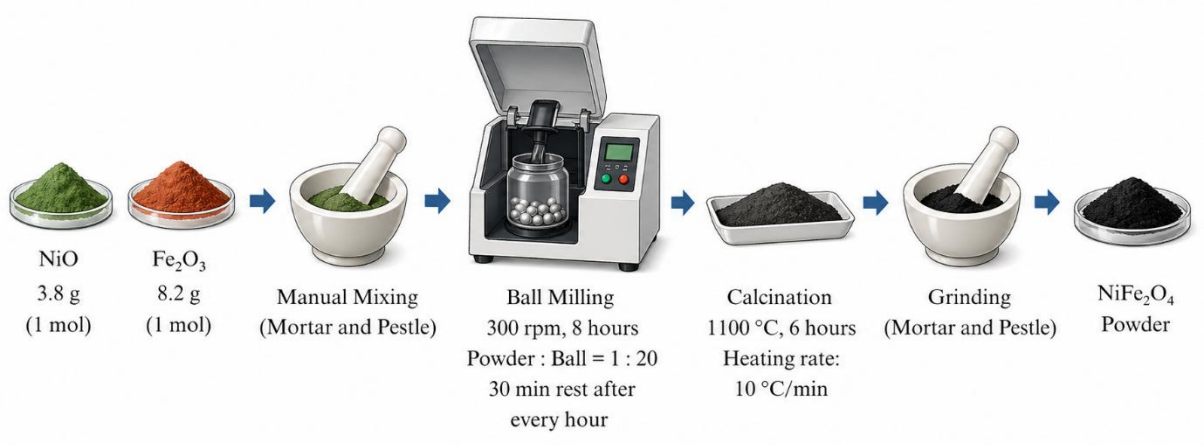


Figure 3. Preparation Process of Nickel Ferrite ($NiFe_2O_4$) Powder by Ball Milling and Calcination

### 2.4 Preparation of TiCN/$NiFe_2O_4$ Composite Paste

The TiCN/$NiFe_2O_4$ composite paste was prepared by mixing TiCN powder, synthesized $NiFe_2O_4$ powder, PVP binder, and ethanol solvent. The powders were manually mixed until a homogeneous composite mixture was obtained. Ethanol was added gradually to improve paste dispersion and produce a suitable consistency for the screen-printing process. The presence of fine TiCN particles obtained from the ball milling process was expected to improve the interaction between TiCN and $NiFe_2O_4$ particles in the composite structure. This condition may contribute to better conductive pathways and more uniform electromagnetic behaviour in the fabricated antenna layer [12], [13]. The composite paste preparation process is shown in Figure 4.



Figure 4. TiCN/$NiFe_2O_4$ composite paste using PVP binder and ethanol solvent.

### 2.5 Fabrication of TiCN/$NiFe_2O_4$ Composite Based MPA

The MPA was fabricated using a screen-printing method an RT Duroid 5880 substrate with a dielectric constant ($\varepsilon r$) of 2.2 and a loss tangent ($\tan \delta$) of 0.0009. Before the composite layer was deposited, the substrate was prepared by removing the unwanted copper layer from one side of the substrate using $FeCl_3$ etching solution. The substrate was immersed in the etching solution until the copper layer was completely removed, followed by cleaning and drying. The substrate preparation process is shown in Figure 5. After substrate preparation, the TiCN/$NiFe_2O_4$ composite paste was deposited onto the substrate surface using the screen-printing technique to form the radiating patch structure. The printed antenna was dried to remove excess solvent and improve the stability of the conductive composite layer. A SubMiniature version A (SMA) connector was then attached to the feeding port region to enable microwave signal transmission during measurement. The fabricated TiCN/$NiFe_2O_4$ composite based MPA is shown in Figure 6.

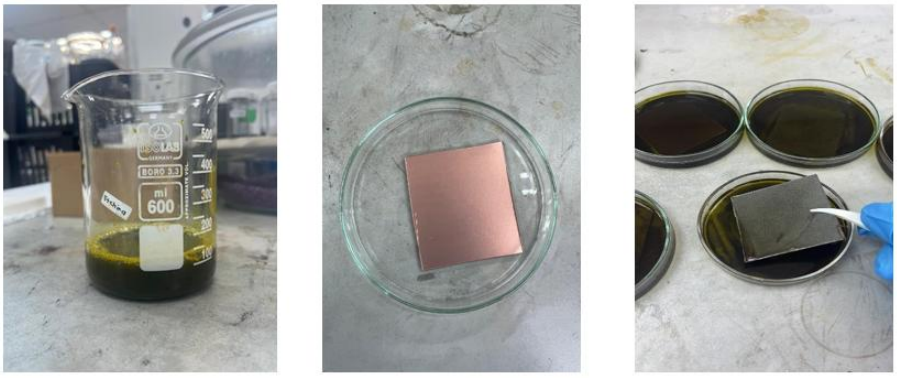



Figure 5. Substrate etching process using $FeCl_3$ solution before antenna fabrication

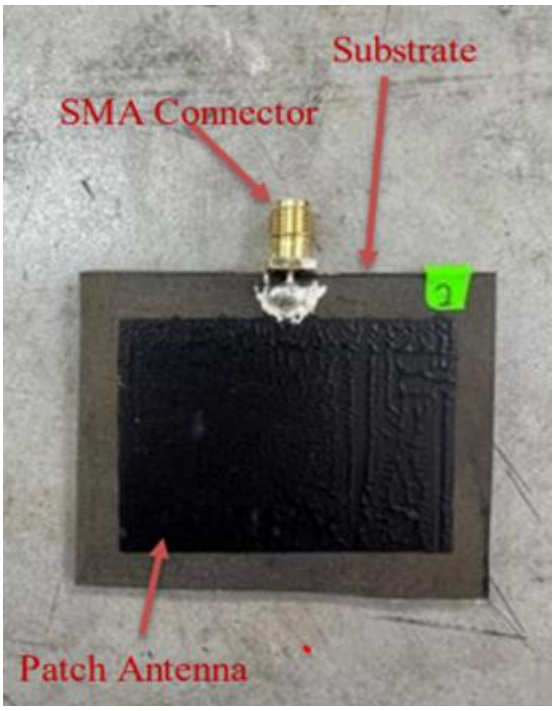



Figure 6. Fabricated TiCN/$NiFe_2O_4$ composite based Microstrip Patch Antenna (MPA)

### 2.6 Characterization Techniques

The structural, morphological, surface, thermal, and electromagnetic properties of the prepared samples were analyzed using several characterization techniques. Particle size distribution of TiCN powder was measured using a Particle Sizer. The phase formation and crystallinity of $NiFe_2O_4$ and TiCN/$NiFe_2O_4$ composite samples were analyzed using X-ray Diffractometer (XRD). The chemical bonding and functional groups were examined using Fourier-transform Infrared Spectroscopy (FTIR). The surface morphology and particle distribution were observed using Scanning Electron Microscope (SEM). Surface area and pore characteristics were measured using Brunauer-Emmet-Teller (BET) analysis. Thermal stability was evaluated using Thermogravimetric Analysis (TGA). The antenna performance was measured using VNA based on return loss and bandwidth characteristics.

## 2.7 Adhesion Test

An adhesion test was conducted to evaluate the attachment strength between the TiCN/$NiFe_2O_4$ composite layer and the substrate surface. Adhesive tape was applied directly onto the printed conductive patch surface and then removed from the substrate. The condition of the composite layer was observed after tape removal to identify any peeling, cracking, or detachment. Good adhesion is important to maintain stable conductivity, surface uniformity, and structural integrity during antenna handling and VNA measurement. The adhesion test process is shown in Figure 7.

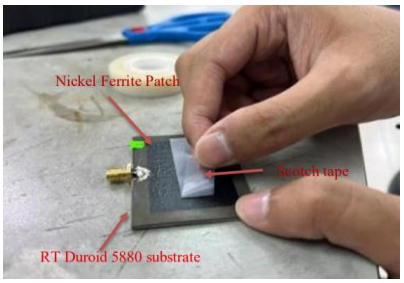



Figure 7. Adhesion test of the fabricated TiCN/$NiFe_2O_4$ composite patch antenna

## 2.8 VNA Measurement

The electromagnetic performance of the fabricated TiCN/$NiFe_2O_4$ composite based MPA was evaluated using a VNA within the frequency range of 5 to 20 GHz. The fabricated antenna was connected to the VNA through the SMA connector, and the reflection coefficient was recorded as the S11 parameter. The return loss performance was used to determine the impedance matching behaviour of the antenna, while the bandwidth was obtained from the frequency range below the -10 dB return loss threshold. The VNA measurement setup is shown in Figure 8. The electromagnetic characterization performed in this study was limited to reflection coefficient analysis using VNA measurement in order to investigate the influence of composite material properties on impedance matching behaviour.




Figure 8. VNA measurement setup for TiCN/$NiFe_2O_4$ composite based MPA

## 3. Results and Discussion

### 3.1 Effect of Ball Milling on TiCN Particle Size Distribution

The particle size distribution of TiCN powder was analyzed to evaluate the effect of the ball milling process on particle refinement. The obtained particle size distribution is summarized in Table 2. The initial TiCN powder showed a relatively large average particle size of approximately 887.3 nm. After the ball milling process, the particle size decreased significantly to a range between approximately 278 nm and 297 nm. The reduction in particle size was mainly caused by repeated collision, compression, and fracture between the steel balls and TiCN particles during the milling process. Prolonged milling duration provided higher mechanical energy, which increased particle fragmentation and produced finer particle distribution [14].

Table 2. Particle size distribution of TiCN samples based on ball milling duration

| Sample | Z-Avg (nm) | Pk 1 Avg (nm) |
|---|---|---|
| 1 | 887.3 | 1022.0 |
| 2 | 286.2 | 360.1 |
| 3 | 278.9 | 305.1 |
| 4 | 297.4 | 365.2 |
| 5 | 282.3 | 318.7 |

The results also showed that longer milling duration generally improved particle refinement compared to the untreated TiCN powder. The smallest average particle size was obtained for Sample 3 with an average particle size of approximately 278.9 nm. However, slight fluctuations in particle size distribution were observed at longer milling durations, which may be related to partial particle agglomeration during prolonged milling process. Despite the slight variation, all milled samples demonstrated significantly smaller particle sizes compared to the as-milled TiCN sample. The reduction in TiCN particle size is important because finer particles may improve the homogeneity of the TiCN/$NiFe_2O_4$ composite structure. The reduction in particle size after prolonged ball milling may increase the effective surface contact area between TiCN particles, thereby improving conductive continuity within the composite structure. Improved particle homogeneity may contribute toward more stable current distribution across the radiating patch layer.Better particle distribution can increase conductive interaction between TiCN particles and improve electromagnetic response within the fabricated composite layer. Smaller particles may also contribute toward more stable current distribution and improved microwave propagation during antenna operation. Therefore, the ball milling process played an important role in improving the structural characteristics of TiCN before composite fabrication.

### 3.2 Phase Formation and Crystallinity Analysis using XRD

The crystal structure and phase formation of the samples were analyzed using the XRD. The diffraction patterns are presented in Figure 9, while the crystallite size and lattice parameters are calculated using the Scherrer equation [15]:

$$D = \frac{K\lambda}{\beta \cos\theta}$$

D is the crystallite size, K is the shape factor, λ is the X-ray wavelength, β is the full width at half maximum, and θ is the bragg angle.

From Figure 9, distinct diffraction peaks can be clearly observed for the calcined sample. These peaks correspond to the characteristic planes of $NiFe_2O_4$, which confirms the successful formation of the spinel ferrite structure after the calcination process. The peaks in the calcined sample appear sharper and more intense compared to the as-calcined sample. This observation indicates an improvement in crystallinity after heat treatment. The sharper diffraction peaks observed after calcination indicate improved structural ordering and enhanced crystal stability within the $NiFe_2O_4$ phase.
The crystallite size calculated using the Scherrer equation shows a clear increase after calcination [16]. As listed in Table 3, the crystallite size increased from about 18.42 nm to 65.05 nm. This increase is caused by grain growth at high temperature. During calcination at 1100 °C, smaller crystallites combine and form larger and more ordered crystal domains [17]. The increase in crystallite size and the sharper diffraction peaks indicate that the material has become more crystalline and stable. The successful formation of the spinel ferrite phase also shows that the synthesis method is effective and suitable for producing the desired material [18]. The absence of significant impurity peaks further suggests that the solid-state synthesis route successfully produced phase-pure spinel ferrite $NiFe_2O_4$.

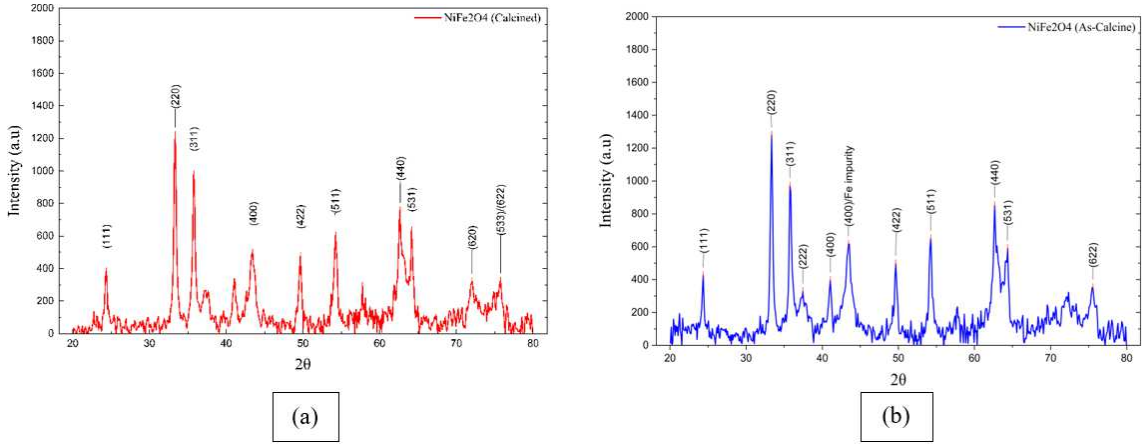



Figure 9 XRD pattern of calcined (a) and as-calcined (b) nickel ferrite

Table 3. Average crystallite size and lattice parameter of the samples

| Sample Condition | 2θ (°) | FWHM (°) | Crystallite Size (nm) | Lattice Parameter (Å) |
|---|---|---|---|---|
| As-calcined | 35.75 | 0.452 | 18.42 | 8.34 |
| Calcined | 35.76 | 0.128 | 65.05 | 8.34 |

### 3.3 Functional Group and Bonding Analysis using Fourier-transform Infrared Spectroscopy (FTIR)

The chemical bonding and functional groups of the samples were analyzed using FTIR. The FTIR spectra are presented in Figure 10. Several absorption peaks can be observed, with the most important peaks located at around 607 $cm^{-1}$ and 419 $cm^{-1}$. These peaks are related to the metal oxygen vibration in the ferrite structure. The peak near 607 $cm^{-1}$ corresponds to the stretching vibration of metal oxygen bonds in the tetrahedral site, while the peak near 419 $cm^{-1}$ is related to the octahedral site in the spinel ferrite structure.

The presence of these two characteristic peaks confirms the formation of nickel ferrite with a spinel structure. The stable metal-oxygen bonding observed in the FTIR spectra indicates good structural integrity after the calcination process. The positions of these peaks are consistent with reported values for ferrite materials, which further supports the validity of the synthesis process. The intensity and clarity of the peaks also indicate that the bonding structure is well formed after calcination. A strong and stable bonding structure is important because it ensures that the material has consistent chemical properties [19]. This result is also in agreement with the XRD analysis, which confirms the formation of the ferrite phase.

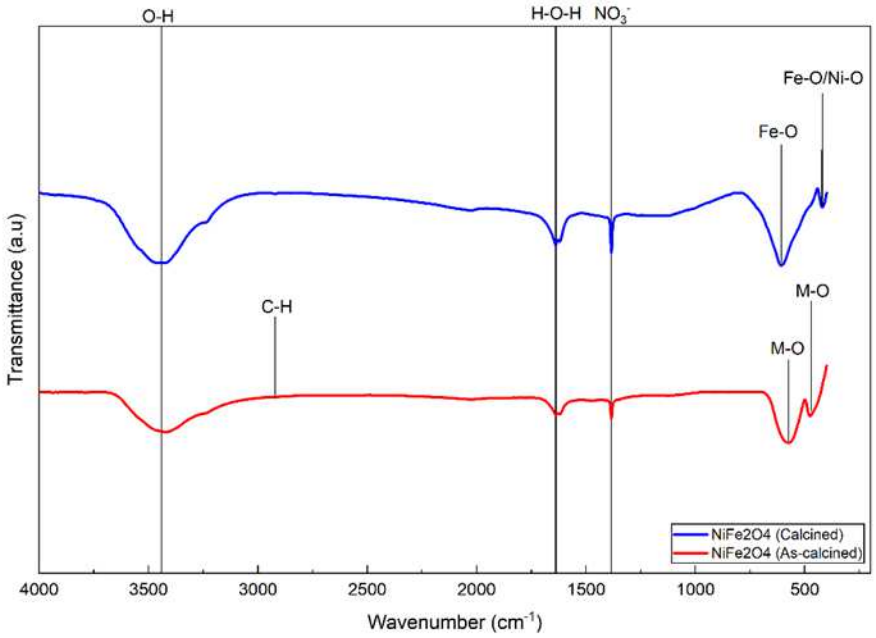



Figure 10 FTIR spectra of nickel ferrite

### 3.4 Morphological Analysis using Scanning Electron Microscope

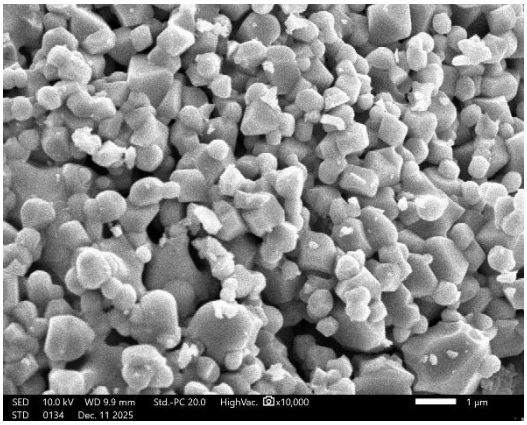
The surface morphology and particle size of the samples were observed using the SEM. The SEM images and particle size distribution are shown in Figure 11, while the average particle size values are listed in Table 4. From Figure 11(a), the calcined nickel ferrite sample shows particles with a relatively uniform shape and an average size of about 95.30 nm. The particles appear clearly defined, which indicates that the calcination process has improved the particle structure. In Figure 11(b), the as-calcined sample shows less defined particles, which suggests that the structure is not fully developed before heat treatment.

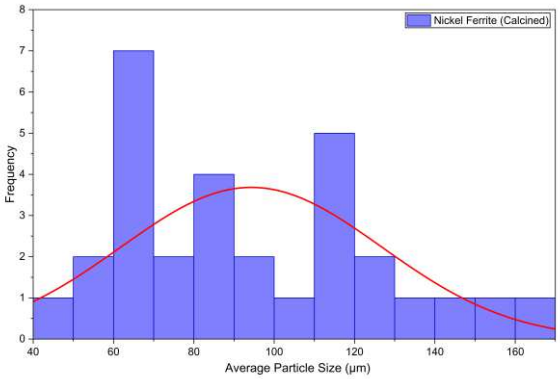
In Figure 11(c), the TiCN-$NiFe_2O_4$ composite shows smaller particles with an average size of about 72.34 nm. The reduction in particle size in the composite sample indicates that the ball milling and mixing process helps to refine the particle structure. The particles also appear more evenly distributed, which shows that the mixing between TiCN and $NiFe_2O_4$ is successful. The improved particle distribution may contribute toward more uniform electromagnetic interaction throughout the conductive composite layer. The comparison between the samples shows that calcination improves particle definition, while the composite formation leads to smaller and more uniform particles. A uniform and fine particle structure is important because

it helps to improve the consistency and quality of the material. This condition is beneficial for applications that require stable structural and physical properties.

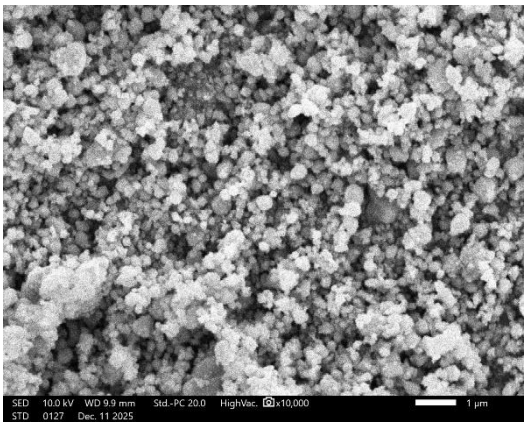
SEM Nickel Ferrite Morphology Particle Size distribution

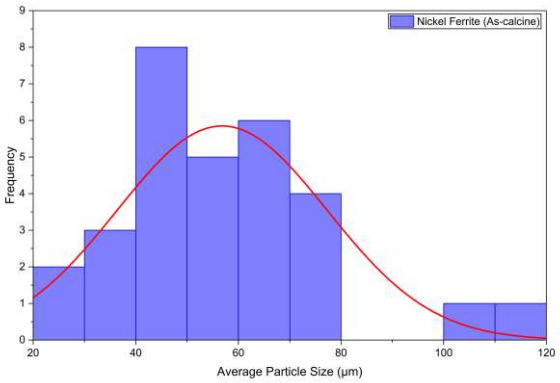
(a)



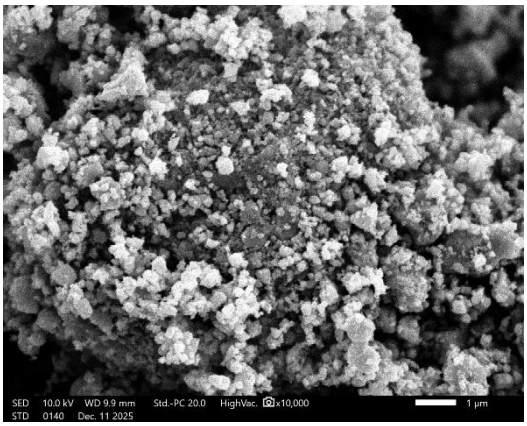




(b)




(c)



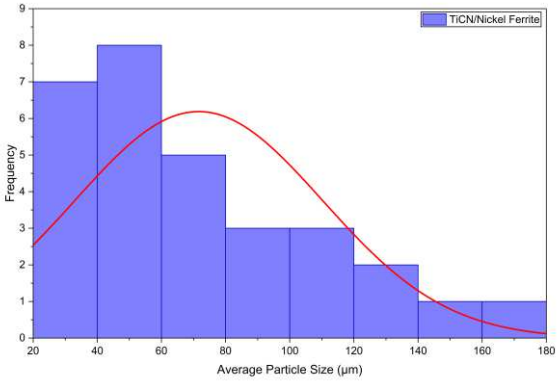




Figure 11 SEM images and particle size distribution of (a) calcined nickel ferrite (b) as-calcined nickel ferrite (c)TiCN/nickel ferrite

Table 4. Average particle size of SEM samples

| Sample ID | Average Particle Size (nm) |
|---|---|
| Calcined Nickel Ferrite | 95.30 |
| As-Calcined Nickel Ferrite | 57.90 |
| TiCN/Nickel Ferrite | 72.34 |

### 3.5 Surface Area and Porosity Analysis using BET

The surface area and porosity of the samples were analyzed using the BET analysis. The adsorption and desorption isotherms are presented in Figure 12, while the calculated surface area values are summarized in Table 6. From Table 5, the surface area of the as-calcined sample is about 34.89 $m^2\ g^{-1}$. After the calcination process, the surface area decreases significantly to about 6.81 $m^2\ g^{-1}$. This large reduction in surface area indicates that structural changes occur during heat treatment.

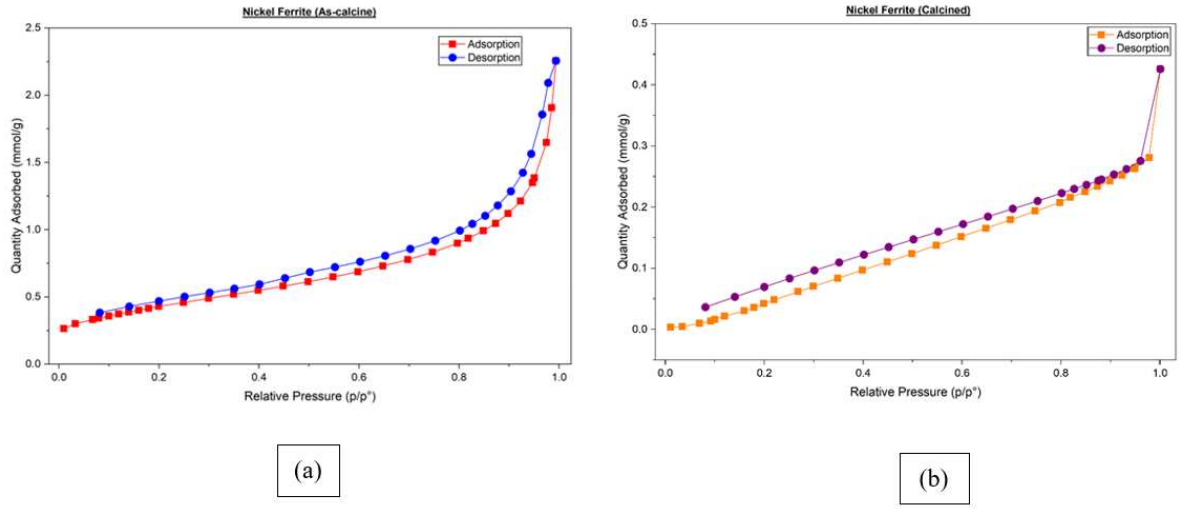



Figure 12 Adsorption-desorption isotherms for (a) as-calcined & calcined nickel ferrite

Table 5. BET Data Analysis

| Sample ID | Condition | BET Surface Area $(m^2/g)$ | Total Pore Volume $(cm^3/g)$ | Average Pore Diameter $(nm)^a$ |
|---|---|---|---|---|
| Sample 1 | as-calcined (Precursor) | 34.89 | 0.0799 | 10.20 |
| Sample 2 | calcined (1100 °C) | 6.81 | 0.0146 | 4.65 |

The isotherm curves shown in Figure 12(a) for the as-calcined sample indicate a higher adsorption volume, which reflects a larger surface area and higher porosity. In contrast, Figure 12(b) for the calcined sample shows a lower adsorption volume, which confirms the reduction in surface area and pore structure after calcination. The decrease in surface area is mainly caused by particle growth and densification during the calcination process. At high temperature, smaller particles combine to form larger particles, which reduces the total surface area. At the same time, pore structures collapse or become less significant, which reduces the

overall porosity of the material. The reduction in surface area and porosity indicates that the material becomes denser and more compact after calcination. The formation of a denser structure may improve the mechanical and thermal stability of the composite material during microwave operation. A denser structure is important because it can improve the stability and mechanical strength of the material. This result is also consistent with the XRD and SEM analysis, which show an increase in crystallite size and particle size after heat treatment.

### 3.6 Thermal Stability Analysis using TGA

The thermal stability of the samples was evaluated using thermogravimetric analysis. The TGA curves for the as-calcined and calcined samples are shown in Figure 13. From Figure 13(a), the as-calcined sample shows a small weight loss at lower temperature. This weight loss is mainly due to the removal of moisture and residual compounds present in the sample. As the temperature increases, the weight loss becomes very minimal, which indicates that the material is relatively stable. For the calcined sample shown in Figure 13(b), the weight loss is even lower compared to the as-calcined sample. The curve shows that there is almost no significant weight change above 200 °C. This result indicates that the calcined material has high thermal stability. The improved thermal stability of the calcined sample is due to the formation of a well-developed crystal structure during the heat treatment process. The removal of volatile components and the formation of stable metal oxygen bonds contribute to the stability of the material at higher temperature. High thermal stability is important for applications that involve elevated temperature conditions. A stable material can maintain structural integrity and performance without significant degradation. This result confirms that the synthesized material is suitable for advanced applications that require thermal resistance. Improved thermal stability is important to maintain stable antenna performance during prolonged high-frequency operation.

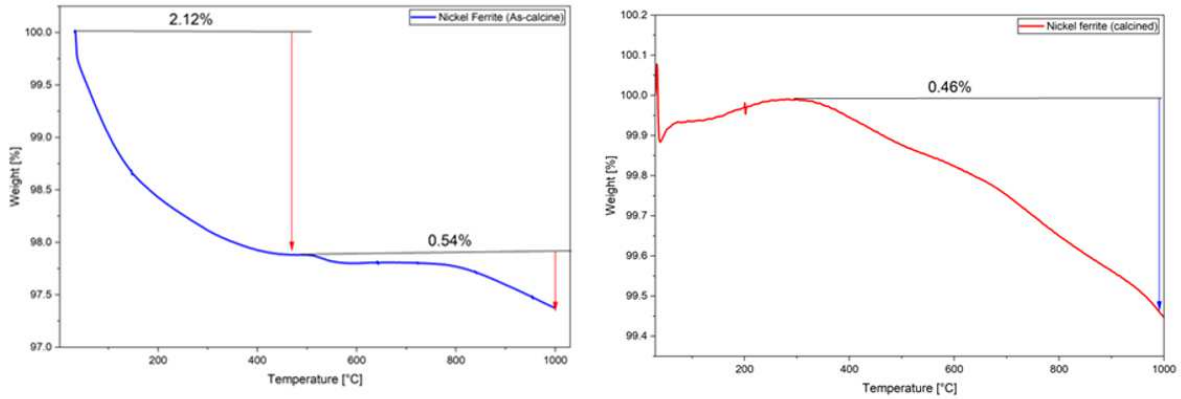


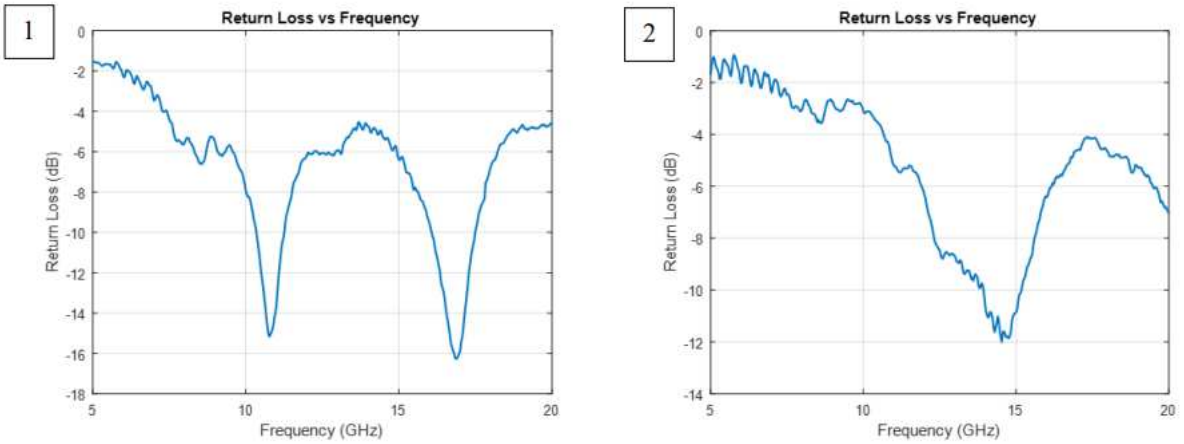

Figure 13 Graph of TGA analysis for nickel ferrite samples (a) as-calcined (b) calcined

The present investigation emphasizes the influence of TiCN particle refinement and composite homogeneity on the impedance matching behaviour and microwave response of the fabricated antenna structures. Therefore, the electromagnetic evaluation in this work mainly focuses on return loss and bandwidth characteristics as preliminary indicators of microwave performance.

### 3.7 Return Loss Analysis

The return loss performance of the fabricated TiCN/$NiFe_2O_4$ composite based MPA was evaluated using a VNA within the frequency range of 5 to 20 GHz. The return loss graph obtained from the S11 parameter is presented in Figure 14, while the return loss values are summarized in Table 6. Different resonance frequencies and return loss behaviours were observed among the fabricated samples due to differences in TiCN particle distribution after the ball milling process.

Sample 1 showed the weakest performance with return loss slightly below -10 dB, which indicated weaker impedance matching. As the TiCN milling duration increased, the antenna performance gradually improved. Sample 4 achieved the best return loss performance with a minimum return loss value of -42.94 dB at 12.53 GHz, indicating excellent impedance matching and efficient microwave signal transmission. In addition, Sample 5 demonstrated dual band resonance behaviour at approximately 7.60 GHz and 13.07 GHz. The dual-band resonance behaviour suggests the existence of multiple electromagnetic interaction pathways within the TiCN/$NiFe_2O_4$ composite layer. The improved antenna performance was mainly influenced by finer TiCN particle distribution, which contributed toward better conductive interaction and more stable current propagation within the composite structure. The improved return loss performance may be associated with enhanced conductive interaction resulting from finer TiCN particle distribution within the composite structure. Improved conductive pathways may reduce reflection losses and improve impedance matching behaviour during microwave propagation.The results confirmed that the TiCN/$NiFe_2O_4$ composite material possesses strong potential for high frequency microwave antenna applications within X band and Ku band frequency regions.



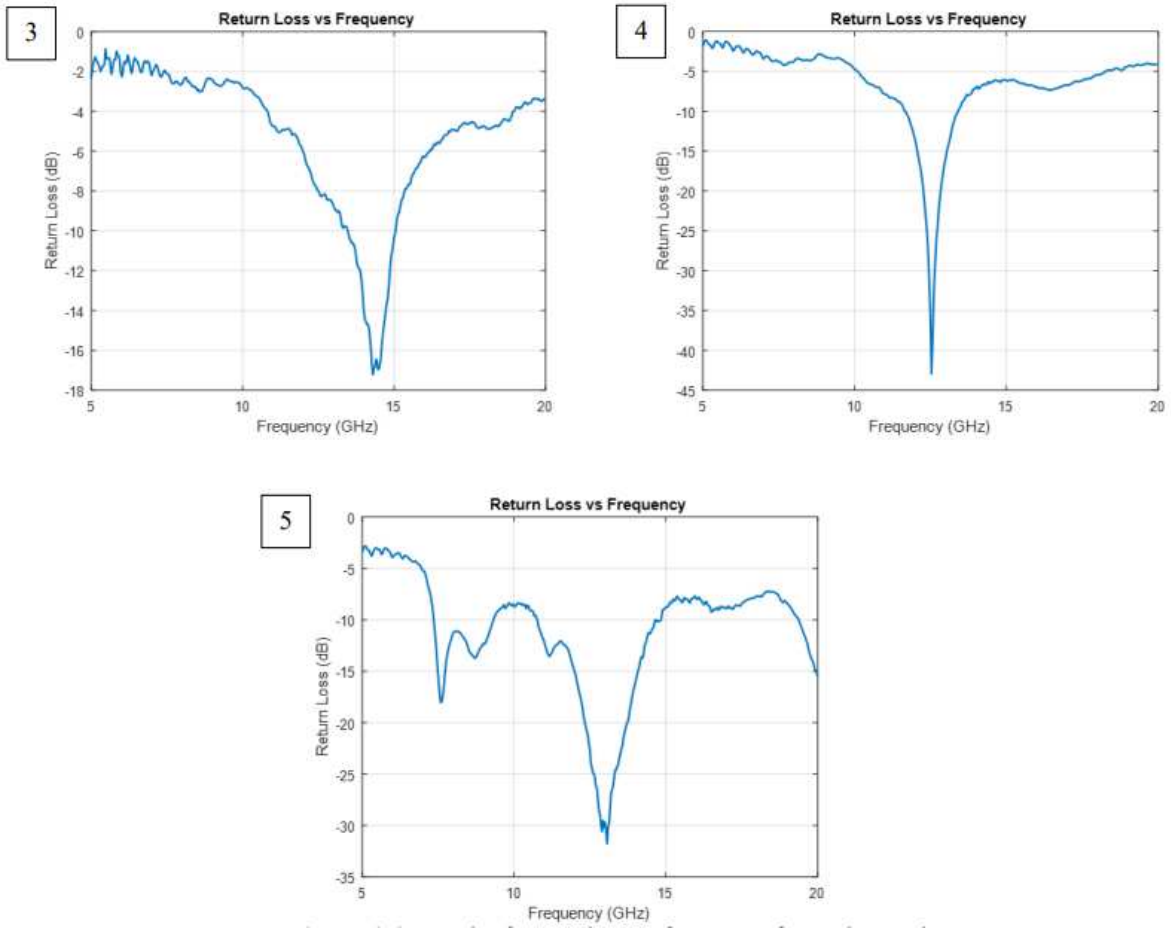



Figure 14 Return loss versus frequency graph of fabricated TiCN/$NiFe_2O_4$ composite based MPAs

Table 6 Return loss performance of fabricated TiCN/$NiFe_2O_4$ composite based MPAs

| Sample | Sample Composition/Processing Condition | Resonance Frequency (GHz) | Return Loss (dB) | Performance Quality |
|---|---|---|---|---|
| 1 | TiCN/NF (as-mill TiCN) | 10.76<br>16.86 | -15.16<br>-16.26 | Dual-band,<br>Good |
| 2 | TiCN/NF (TiCN milled 2 hours) | 14.53 | -12.00 | Acceptable |
| 3 | TiCN/NF (TiCN milled 4 hours) | 14.3 | -17.22 | Good |
| 4 | TiCN/NF (TiCN milled 6 hours) | 12.53 | -42.94 | Excellent |
| 5 | TiCN/NF (TiCN milled 8 hours) | 7.60<br>13.06 | -18.05<br>-31.76 | Dual-band,<br>Excellent |

### 3.8 Bandwidth Analysis

The bandwidth performance of the fabricated TiCN/$NiFe_2O_4$ composite based MPA was evaluated based on the frequency range below the -10 dB return loss threshold. The bandwidth measurement for each fabricated sample is presented in Figure 15, while the corresponding bandwidth values are summarized in Table 7. The obtained results showed that all fabricated antennas achieved bandwidth values greater than 0.87 GHz, indicating successful microwave operation within high frequency regions. Sample 1 demonstrated the narrowest bandwidth due to weaker impedance matching and less uniform conductive distribution within the composite structure. As the TiCN milling duration increased, the bandwidth performance gradually improved. Sample 4 achieved a bandwidth value of 1.70 GHz at 12.53 GHz, while Sample 5 demonstrated the best overall bandwidth performance with dual band operation at approximately 7.60 GHz and 13.07 GHz. The wider bandwidth observed in Sample 5 indicated stronger electromagnetic interaction between TiCN conductive particles and $NiFe_2O_4$ magnetic particles within the composite layer. The synergistic interaction between conductive TiCN and magnetic $NiFe_2O_4$ phases may contribute toward broader impedance matching characteristics and improved microwave propagation. The obtained bandwidth results confirmed that the fabricated TiCN/$NiFe_2O_4$ composite based MPA possesses strong potential for microwave communication applications involving X band and Ku band frequency regions.

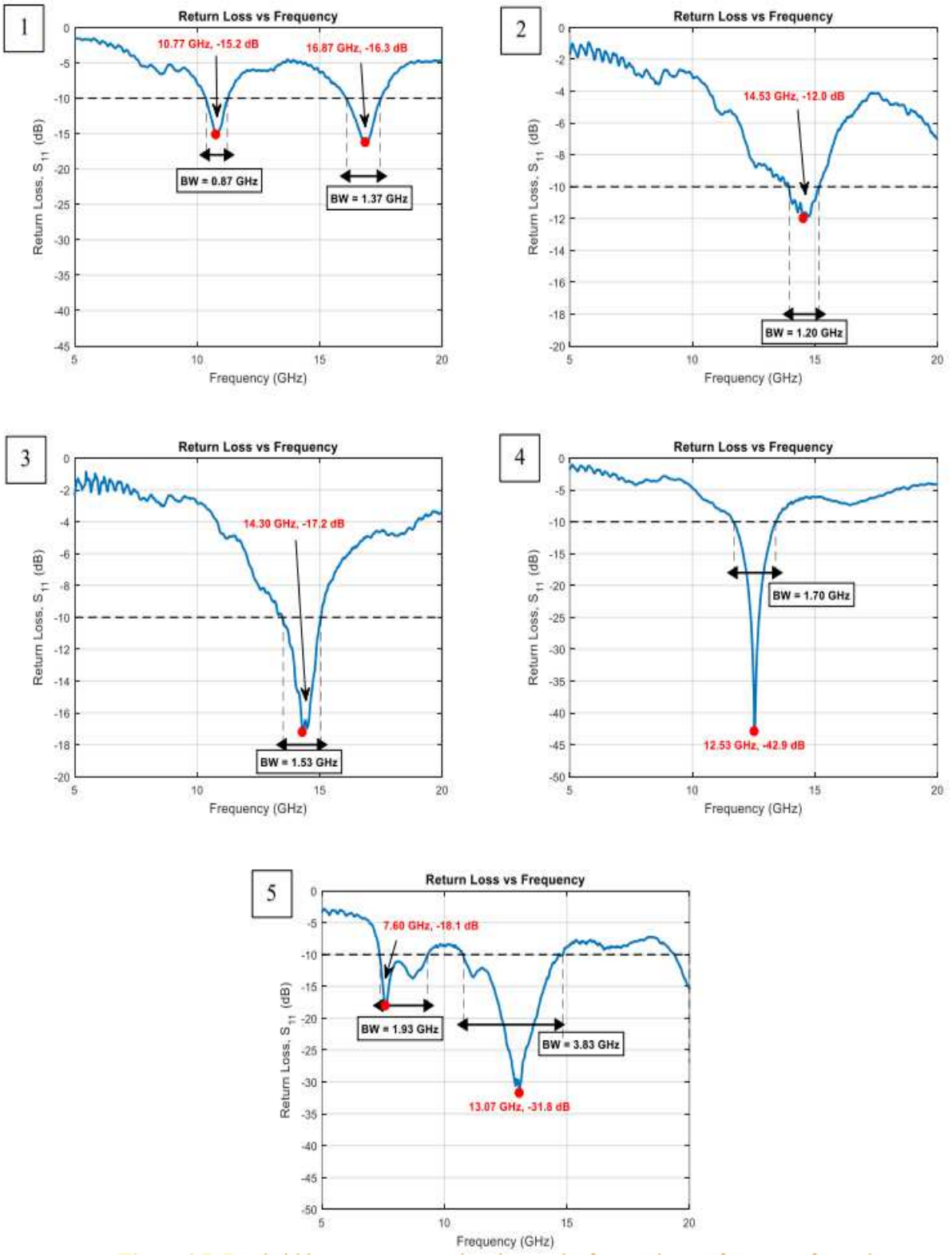



Figure 15 Bandwidth performance of fabricated TiCN/$NiFe_2O_4$ composite based MPAs

Table 7. Bandwidth performance of fabricated TiCN/$NiFe_2O_4$ composite based MPAs

| Sample | Sample Composition/Processing Condition | Resonance Frequency (GHz) | Return Loss (dB) | Bandwidth (GHz) | Performance |
|---|---|---|---|---|---|
| 1 | TiCN/NF (as-mill TiCN) | 10.77<br>16.87 | -15.20<br>-16.30 | 0.87<br>1.37 | Dual-band, Narrow BW |
| 2 | TiCN/NF (TiCN milled 2 hours) | 14.53 | -12.00 | 1.20 | Narrowest BW |
| 3 | TiCN/NF (TiCN milled 4 hours) | 14.30 | -17.20 | 1.53 | Moderate BW |
| 4 | TiCN/NF (TiCN milled 6 hours) | 12.53 | -42.90 | 1.70 | High-Q, Moderate BW |
| 5 | TiCN/NF (TiCN milled 8 hours) | 7.60<br>13.07 | -18.10<br>-31.80 | 1.93<br>3.83 | Dual-band, Widest BW |

### 3.9 Effect of Ball Milling Duration on Antenna Performance

Ball milling duration significantly influenced the electromagnetic performance of the fabricated TiCN/$NiFe_2O_4$ composite based MPA. The particle size analysis discussed in Section 3.1 showed that prolonged ball milling process reduced the TiCN particle size and improved particle distribution within the composite structure. Better particle homogeneity contributed toward improved conductive pathways and more stable microwave signal propagation across the radiating patch surface. The overall electromagnetic performance of the fabricated antennas is summarized in Table 8. The obtained results showed that samples with finer TiCN particle distribution generally demonstrated improved return loss and bandwidth performance. Sample 4 achieved the best return loss value of -42.94 dB, while Sample 5 demonstrated the widest bandwidth together with dual band operation. Although Sample 3 exhibited the smallest average particle size, the antenna performance was also influenced by particle distribution uniformity and conductive interaction within the composite structure. Overall, prolonged ball milling duration improved the electromagnetic behaviour of the fabricated TiCN/$NiFe_2O_4$ composite based MPA by enhancing composite homogeneity and operating frequency response within X band and Ku band regions.

Table 8. Overall electromagnetic performance of fabricated TiCN/$NiFe_2O_4$ composite based MPAs

| Sample | Composition | Frequency (GHz) | Return Loss (dB) | Bandwidth (GHz) | Frequency Band |
|---|---|---|---|---|---|
| 1 | As-mill TiCN + | 10.77 | -15.20 | 0.87 | X/Ku |
| | Calcined NF | 16.87 | -16.30 | 1.37 | |
| 2 | 2h TiCN + | 14.53 | -12.00 | 1.20 | Ku |
| | Calcined NF | | | | |
| 3 | 4h TiCN + | 14.30 | -17.20 | 1.53 | Ku |
| | Calcined NF | | | | |
| 4 | 6h TiCN + | 12.53 | -42.90 | 1.70 | Ku |
| | Calcined NF | | | | |
| 5 | 8h TiCN + | 7.60 | -18.10 | 1.93 | C/Ku |
| | Calcined NF | 13.07 | -31.80 | 3.83 | |

## 4. Conclusion

TiCN/$NiFe_2O_4$ composite materials were successfully developed for high frequency MPA applications through ball milling, calcination, and composite fabrication processes. The ball milling process significantly reduced the TiCN particle size and improved particle distribution within the composite structure. XRD and FTIR analyses confirmed the successful formation of spinel $NiFe_2O_4$ structure, while SEM analysis demonstrated improved particle homogeneity after composite formation. BET and TGA analyses showed that the synthesized material possessed good structural stability and thermal resistance after calcination process. The fabricated TiCN/$NiFe_2O_4$ composite based MPA demonstrated promising microwave performance within the frequency range of 5 to 20 GHz. Sample 4 achieved the best return loss performance of -42.94 dB at 12.53 GHz, while Sample 5 demonstrated the widest bandwidth together with dual band operation. The obtained results confirmed that prolonged ball milling duration improved the electromagnetic performance of the fabricated antenna through better conductive interaction and improved composite homogeneity. The present work primarily emphasizes material development and preliminary electromagnetic characterization of TiCN/$NiFe_2O_4$ composite-based microstrip patch antennas. Detailed radiation pattern, gain, and antenna efficiency investigations may be further explored in future studies to provide a more comprehensive antenna performance evaluation. Overall, the fabricated TiCN/$NiFe_2O_4$ composite material demonstrated strong potential for high frequency microwave antenna applications within X band and Ku band frequency regions. The findings demonstrate that particle refinement through ball milling plays an important role in determining the electromagnetic behaviour of TiCN/$NiFe_2O_4$ composite-based antennas.

The present work provides preliminary insight into the relationship between composite microstructure and microwave antenna performance within X-band and Ku-band frequency regions.

## Declaration of Competing Interest

The authors declare that they have no known competing financial interests or personal relationships that could have appeared to influence the work reported in this paper.

**Acknowledgements**

The authors would like to acknowledge with gratitude the financial support received from Universiti Malaysia Pahang Al-Sultan Abdullah (UMPSA) (Ref. RDU233309).

**Authors Contribution**

All authors contributed to the study conception and design. Material preparation, data collection and analysis were performed by C. D. F. C. Fadzrizal, N. I. Z. Azman, and M. A. Jusoh. The first draft of the manuscript was written by C. D. F. C. Fadzrizal and reviewed and edited by N. I. Z. Azman, S. Baudha and M. A. Jusoh. All authors read and approved the final manuscript.

**Data Availability**

The datasets used or analyzed during the current study are available from the corresponding author on reasonable request.

**References**

[1] M. U. Khan, M. S. Sharawi, and R. Mittra, "Microstrip patch antenna miniaturisation techniques: A review," 2015. doi: 10.1049/iet-map.2014.0602.

[2] "Advancements in Microstrip Patch Antennas: The Transformative Role of Nanomaterials in Patch and Substrate Design for Advanced Communication Technology." [Online]. Available: https://ssrn.com/abstract=5072049

[3] R. M. Redzuwan, J. Sampe, R. Latif, Z. A. Rhazali, and N. H. M. Yunus, "Performance analysis of tantalum and copper patches in micro-electro-mechanical systems based microstrip patch antennas for 5th generation mmWave applications," *Advances in Science and Technology Research Journal*, vol. 19, no. 8, pp. 285–295, 2025, doi: 10.12913/22998624/205744.

[4] P. A. M. Mercy, "Novel nanocomposite based microstrip patch antenna for C and X band applications," *Mater. Chem. Phys.*, vol. 326, p. 129593, Oct. 2024, doi: 10.1016/J.MATCHEMPHYS.2024.129593.

[5] Z. Zheng, D. Liu, X. Sun, Y. Wang, H. Zhao, and J. Xu, "Research Progress on Titanium Carbonitride (TiCN) Materials: From Coatings to Nanoparticles for Enhanced Mechanical Property and Corrosion Protection: A Review," Mar. 01, 2026, *Multidisciplinary Digital Publishing Institute (MDPI)*. doi: 10.3390/coatings16030316.

[6] Y. Ma, Y. Jiang, C. Wang, S. Kang, G. Chen, and B. Zhong, "Microwave absorption performance enhancement of NiFe2O4/GNs composite with hollow hexagonal-like structure," *J. Magn. Magn. Mater.*, vol. 565, 2023, doi: 10.1016/j.jmmm.2022.170281.

[7] Z. Zhang, Y. Liu, G. Yao, G. Zu, and Y. Hao, "Synthesis and characterization of NiFe2O4 nanoparticles via solid-state reaction," *Int. J. Appl. Ceram. Technol.*, vol. 10, no. 1, 2013, doi: 10.1111/j.1744-7402.2011.02719.x.

[8] A. Baykal, N. Kasapoğlu, Y. Köseoğlu, M. S. Toprak, and H. Bayrakdar, "CTAB-assisted hydrothermal synthesis of NiFe2O4 and its magnetic characterization," *J. Alloys Compd.*, vol. 464, no. 1–2, 2008, doi: 10.1016/j.jallcom.2007.10.041.

[9] V. F. Tarţa, I. Chicinaş, T. F. Marinca, B. V. Neamţu, F. Popa, and C. V. Prică, "Synthesis of the nanocrystalline/nanosized NiFe2O4 powder by ceramic method and mechanical milling," in *Solid State Phenomena*, 2012. doi: 10.4028/www.scientific.net/SSP.188.27.

[10] H. Yang, X. Zhang, W. Ao, and G. Qiu, "Formation of NiFe2O4 nanoparticles by mechanochemical reaction," *Mater. Res. Bull.*, vol. 39, no. 6, 2004, doi: 10.1016/j.materresbull.2004.02.001.

[11] Z. Kong, Z. Wang, B. Chen, Y. Li, and R. Li, "Effect of Ball Milling Time on the Microstructure and Properties of High-Silicon–Aluminum Composite," *Materials*, vol. 16, no. 17, 2023, doi: 10.3390/ma16175763.

[12] Z. Zhang, Y. Wang, G. Zu, Z. Cao, J. Liu, and C. Wang, "Effect of TiN content on properties of NiFe2O4-based ceramic inert anode for aluminum electrolysis," *Int. J. Appl. Ceram. Technol.*, vol. 18, no. 4, 2021, doi: 10.1111/ijac.13752.

[13] Z. Zhang and J. Xu, "Sintering kinetics and properties of NiFe2O4-based ceramics inert anodes doped with TiN nanoparticles," *Int. J. Appl. Ceram. Technol.*, vol. 20, no. 1, 2023, doi: 10.1111/ijac.14231.

[14] A. Hajalilou, M. Hashim, R. Ebrahimi-Kahrizsangi, H. Mohamed Kamari, and S. Kanagesan, "Parametric optimization of NiFe2O4 nanoparticles synthesized by mechanical alloying," *Materials Science-Poland*, vol. 32, no. 2, 2014, doi: 10.2478/s13536-013-0173-x.

[15] S. Rahavi, A. Monshi, R. Emadi, A. Doostmohammadi, and H. Akbarian, "Determination of crystallite size in synthetic and natural hydroxyapatite: A comparison between XRD and TEM results," in *Advanced Materials Research*, 2013. doi: 10.4028/www.scientific.net/AMR.620.28.

[16] M. Gharagozlou, "Influence of calcination temperature on structural and magnetic properties of nanocomposites formed by Co-ferrite dispersed in sol-gel silica matrix using tetrakis(2-hydroxyethyl) orthosilicate as precursor," *Chem. Cent. J.*, vol. 5, no. 1, 2011, doi: 10.1186/1752-153X-5-19.

[17] W. Zarai *et al.*, "Effect of Calcination Temperature on Structural and Optical Properties of Mg0.6Co0.4FeAlO4 Spinel Ferrites for Optoelectronic Applications and Non-volatile Organic Memories," *J. Inorg. Organomet. Polym. Mater.*, 2025, doi: 10.1007/s10904-025-03911-4.

[18] A. Monshi, M. R. Foroughi, and M. R. Monshi, "Modified Scherrer Equation to Estimate More Accurately Nano-Crystallite Size Using XRD," *World Journal of Nano Science and Engineering*, vol. 02, no. 03, 2012, doi: 10.4236/wjnse.2012.23020.

[19] Zh. Khamzina, R. Kudaibergenova, and E. Baibazarova, "SYNTHESIS AND CHARACTERIZATION OF NiFe2O4 SPINEL NANOPARTICLES," *Chemical Journal of Kazakhstan*, no. 4, 2024, doi: 10.51580/2024-4.2710-1185.51.